This article has been accepted for publication in a future issue of this journal, but has not been fully edited. Content may change prior to final publication. Citation information: DOI 10.1109/TMI.2017.2673022, IEEE Transactions on Medical Imaging

Visualizing epithelial expression in vertical and horizontal planes with dual axes confocal endomicroscope using compact distal scanner

Gaoming Li, Haijun Li, Xiyu Duan, Quan Zhou, Juan Zhou, Kenn R. Oldham, Thomas D. Wang, *Member, IEEE*

***Abstract*—The epithelium is a thin layer of tissue that lines hollow organs, such as colon. Visualizing in vertical cross-sections with sub-cellular resolution is essential to understanding early disease mechanisms that progress naturally in the plane perpendicular to the tissue surface. The dual axes confocal architecture collects optical sections in tissue by directing light at an angle incident to the surface using separate illumination and collection beams to reduce effects of scattering, enhance dynamic range, and increase imaging depth. This configuration allows for images to be collected in the vertical as well as horizontal plane. We designed a fast, compact monolithic scanner based on the principle of parametric resonance. The mirrors were fabricated using microelectromechanical systems (MEMS) technology and were coated with aluminum to maximize near-infrared reflectivity. We achieved large axial displacements >400 μm and wide lateral deflections >20^{o}. The MEMS chip has a 3.2×2.9 mm^2 form factor that allows for efficient packaging in the distal end of an endomicroscope. Imaging can be performed in either the vertical or horizontal plane with 430 μm depth or 1×1 mm^2 area, respectively, at 5 frames per second. We systemically administered a Cy5.5-labeled peptide that is specific for EGFR, and collected near-infrared fluorescence images ex vivo from pre-malignant mouse colonic epithelium to reveal the spatial distribution of this molecular target. Here, we demonstrate a novel scanning mechanism in a dual axes confocal endomicroscope that collects optical sections of near-infrared fluorescence in either vertical or horizontal planes to visualize molecular expression in the epithelium.**

***Index Terms*—Molecular and cellular imaging, endoscopy, optical imaging, gastrointestinal tract, system design**

This work was supported in part by the National Institutes of Health (NIH) grants R01 CA200007 (TDW), R01 EB020644 (KRO), and R01 CA193377 (TDW) and by gift funds provided by Mary L. Petrovich.

G. Li, H. Li, J. Zhou, and *T.D. Wang are with the Department of Medicine, Division of Gastroenterology, University of Michigan, Ann Arbor, MI 48104 (email: gaomingl@umich.edu, haijunl@umich.edu, juzhou@umich.edu, thomaswa@umich.edu).

X. Duan, Q. Zhou, and *T.D. Wang are with the Department of Biomedical Engineering, University of Michigan, Ann Arbor, MI 48104 (email: dxy@umich.edu, zhouquan@umich.edu).

K.R. Oldham and *T.D. Wang are with the Department of Mechanical Engineering, University of Michigan, Ann Arbor, MI 48104 (email: oldham@umich.edu).

I. Introduction

TABLETOP confocal microscopes collect optical sections in biological tissues with sub-cellular resolution by using a "pinhole" to reject scattered light [1]. Endomicroscopes use the core of a flexible optical fiber instead, and are being adopted in the clinic to provide instantaneous feedback on tissue pathology [2,3]. In these instruments, the objective lens and fiber are aligned along a single axis and provide images in horizontal planes only. The epithelium is a thin, highly metabolic layer of tissue [4] that expresses unique molecular targets that reveal biological function [5], and has dimensions of ~400 μm in the normal condition [6]. Most human cancers originate in the epithelium of hollow organs [7], and extend downward in the vertical direction. An accurate evaluation of the depth of invasion in early lesions is critical for proper therapeutic management [8]. Also, images in the vertical plane can localize the depth of disease relative to the tissue surface. Pathologists use this orientation to assess the extent of cancer invasion [9]. Thus, endomicroscopy is a promising technology for visualizing molecular expression in the epithelium of hollow organs and for guiding physician biopsy [10-12].

In the dual confocal axes configuration, the excitation beam is directed at an angle incident to the tissue surface and uses separate optical paths for illumination and collection [13]. This off-axis geometry minimizes the effects of tissue scattering [14], and enhances the dynamic range of detection so that images can be collected in vertical planes [15]. The region of overlap between the two beams (focal volume) can achieve sub-cellular resolution. Low numerical aperture (NA) lenses are used to provide a long working distance to allow for a miniature scanner to be placed in the post-objective position. This location provides flexibility to use different scanning mechanisms to interrogate biological tissues. Also, a diffraction limited spot can be swept over arbitrarily large fields-of-view (FOV) without optical aberrations. Using this arrangement, the dual axes optical design can be scaled down to millimeter dimensions without loss of resolution. A compact, high speed mirror is needed for scanning, and is the key factor to realizing this new class of endomicroscope.

Previously, electrostatic scanners have been fabricated with compact dimensions using micro-electro-mechanical systems (MEMS) processes. These devices perform fast lateral scanning, but were able to achieve vertical displacements of

This article has been accepted for publication in a future issue of this journal, but has not been fully edited. Content may change prior to final publication. Citation information: DOI 10.1109/TMI.2017.2673022, IEEE Transactions on Medical Imaging

only ~50 μm [16,17], an inadequate result for epithelial imaging. An electrothermal 1D MEMS tunable microlens has been used to achieve a depth scan of over 400 μm but with a slow speed [18]. We have recently developed a miniature scanner actuator that performs both wide lateral deflections and large out-of-plane motion in a monolithic device [19]. We achieved high speeds needed for in vivo imaging using a design is based on the principle of parametric resonance [20]. In this approach, the drive signal is applied at frequencies near $2\omega_o/n$ (ω_o is the natural frequency of vibrational modes and n is an integer ≥1). These scanners are mechanically robust, highly reliable, and fabricated at low cost with high yield. They are a promising alternative to large, bulky actuators found in conventional microscopes, and can be used in an endomicroscope to provide real time horizontal and vertical sectioning capabilities. Here we demonstrate integration of this device into the distal end of a dual axes confocal endomicroscope that is scaled down in dimensions to 5.5 mm diameter, and can be used either as a handheld imaging instrument or as an adjunct to medical endoscopy.

II. METHODS

A. Optical design

We performed ray-trace simulations in non-sequential mode (ZEMAX, ver. 13) to identify commercially-available optics needed to achieve diffraction-limited resolution with a scaled down dual axes confocal scanhead, Fig 1. We aimed to achieve optical sections in vertical planes with a large FOV of 1000 μm laterally and >400 μm axially to image the depth of the epithelium in colon. We used collimated illumination and collection beams focused by a parabolic mirror (focal length, f = 4.6 mm) in a folded optical path with magnification 2.2. The focused beams pass at half-angle of $\alpha = 24.3^o$ through a 1.8 mm diameter fused-silica solid immersion lens (SIL) that has an index of refraction of n = 1.47. Fluorescence emission passes through the SIL reflects off the scanner to the opposite surface of the parabolic mirror.

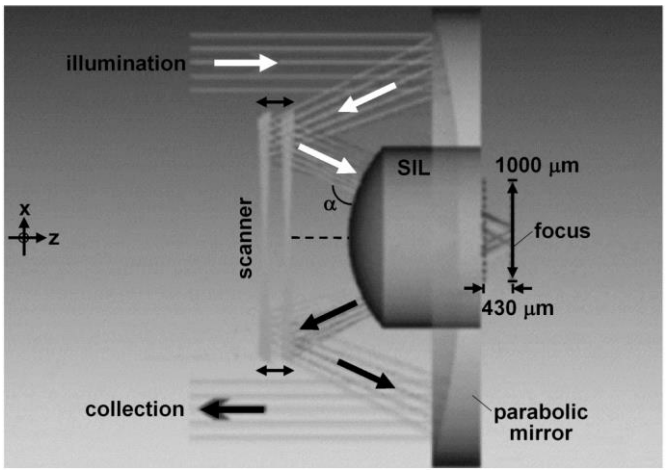

Fig. 1. Optical design of dual axes scanhead. Separate illumination and collection beams are incident at angle to tissue to reduce effects of light scattering and provide high dynamic range for imaging in the vertical plane. Optical path is folded in a zig-zag pattern between scanner and parabolic focusing mirror.

The parabolic mirror (Hanbo Precision-Tech Co, Ltd) is coated with silver (Ag) film to provide >95% reflectivity between 600 and 900 nm to focus the two near-infrared (NIR) beams. The SIL is used as the point of contact for the optics with the tissue surface and to reduce spherical aberrations. The SIL is inserted with a Class II free fit into a 1.8 mm diameter hole located in the center of the parabolic mirror, and is sealed with UV-curable glue (NOA61, Norland).

B. Imaging system

A schematic of the imaging system is shown, Fig. 2. A solid-state diode laser (300 mW, CNI Laser Inc) provides illumination at λ_{ex} = 671 nm. The beam passes through a variable neutral density filter (NDC-50C-4, Thorlabs) and is focused by lens L_1 (f = 15.4 mm, PAF-X-15-PC-B, Thorlabs) into a single mode optical fiber (S630-HP, NA = 0.12, Nufern). The illumination and collection beams are delivered through a pair of custom 1.2 mm diameter fiber-coupled gradient index (GRIN) collimators (GrinTech GmbH) with a center-to-center distance of 3.8 mm. Two Risley prisms are inserted in the illumination path to optimize alignment. The two beams are oriented parallel to the main optical axis of the silver-coated parabolic focusing mirror. The collection collimator delivers NIR fluorescence that is collimated by lens L_2 (f = 18.4 mm, C280TME-B, Thorlabs), and passes through a band pass filter (FF01-716/40-25, Semrock) that transmits from 696-736 nm with >93% efficiency. Lens L_3 (f = 18.4 mm, C280TME-B, Thorlabs) focuses the light onto a photomultiplier tube (PMT, H7422PA-40, Hamamatsu) detector.

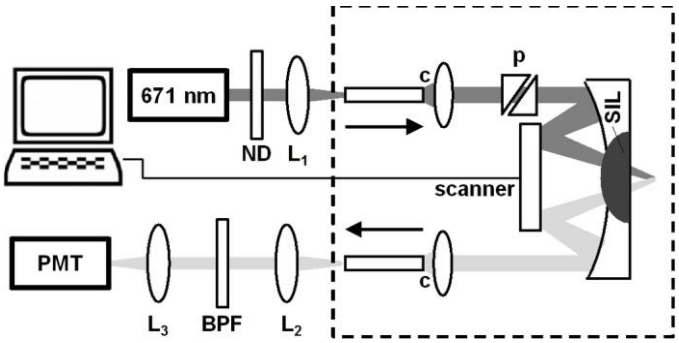

Fig. 2. Schematic of imaging system. Details provided in text. Key: ND: neutral density filter, L_{1-3}: lenses, c: collimators, p: prisms, SIL: solid immersion lens, s: scanner, BPF: bandpass filter, PMT: photomultiplier tube.

C. MEMS scanner

We designed and developed a compact, monolithic electrostatic, 3D micro-electro-mechanical systems (MEMS) scanner with a mirror geometry to match the dual axes architecture based on the principle of parametric resonance, Fig. 3 [19]. Two reflectors with dimensions of 690×700 μm^2 each and thickness of 45 μm are connected by a 1.31 mm strut. The surface is coated with a 70 nm layer of aluminum (Al) for high reflectivity >90% between 400 and 700 nm. The mirror is mounted on a gimbal frame to minimize cross-talk between the X and Y axes and is coupled to a set of inner and outer

This article has been accepted for publication in a future issue of this journal, but has not been fully edited. Content may change prior to final publication. Citation information: DOI 10.1109/TMI.2017.2673022, IEEE Transactions on Medical Imaging

torsional springs that determine the resonance frequencies for horizontal scanning. The gimbal is attached to U-shaped suspensions via serpentine springs located at each corner that determine the resonance frequencies for vertical scanning. This device was fabricated with a deep cavity (high aspect ratio and steep side walls) on the back side of the substrate to allow for large axial displacements using a 3 step deep reactive-ion etch (DRIE) process.

We used electrostatic comb-drive actuators to produce either large axial displacements or wide lateral deflections by tuning the frequency, voltage, and duty cycle of a square wave drive signals. The duty cycle of the excitation can have a significant effect on the performance of the scanner [21]. The scanner can alternate between Z-axis piston and Y-axis tilting modes to "switch" the plane of imaging from vertical to horizontal and vice versa. A dense Lissajous scan pattern is formed that repeats itself at 5 frames per sec, generating images in either the vertical or horizontal plane with dimensions of 400×172 or 400×400 pixels, respectively, at 100% coverage. We etched 4 ellipsoid shaped holes in the substrate (arrow) to reduce weight and minimize air damping effects after packaging.

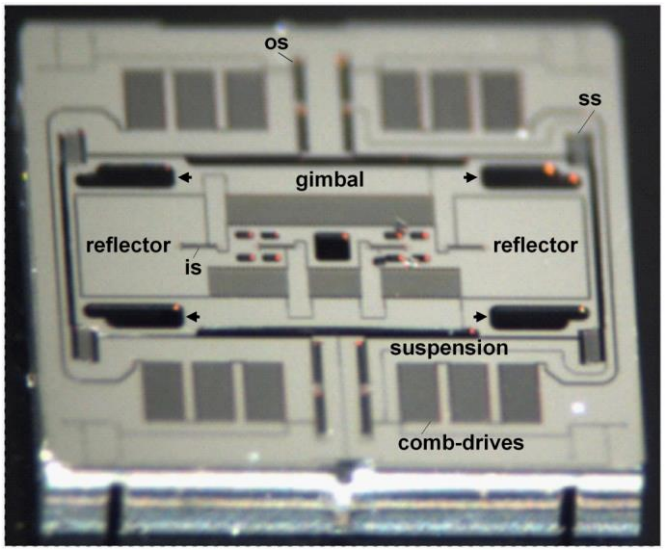

Fig. 3. MEMS scanner. Scanning electron micrograph (SEM) shows a compact, monolithic device mounted on a gimbal frame that is coupled to a set of inner (is) and outer (os) torsional springs and is attached to U-shaped suspensions via serpentine springs (ss). Scanner can switch between wide lateral deflections and large axial displacements determined by parameters of drive signals to comb-drive actuators.

We first characterized the frequency response of the scanner in each axis at ambient temperature and pressure. We used a calibrated position sensing detector (PSD) to measure the out-of-plane displacement and optical scan angle. The scanner was driven at parametric resonance using a pulsed drive voltage at a frequency approximately twice that of each eigenmode. The frequency was swept at various drive voltages and duty cycles using either an upsweep (low-to-high frequency) or downsweep (high-to-low frequency). We empirically adjusted the voltage and duty cycle of the pulsed drive signal to characterize the amplitude and bandwidth of the scanner in each direction. This mapping identifies parameters that can be used to operate the scanner with minimal parasitic vibrations and for different imaging applications with unique deflection amplitudes or scan speeds.

We confirmed the magnitude of the out-of-plane displacement by recording videos at 4000 frames per seconds using a high speed camera (FASTCAM MC2.1, Photron USA, Inc.). We used a 12 bit multi-function data acquisition board (PCI-6115, National Instruments) to digitize the analog signal from the PMT detector and to generate drive signals to the scanner via a 2-channel high voltage amplifier (2350, TEGAM). The system was controlled using custom software (LabVIEW, National Instruments).

D. Scanner packaging

We attached the scanner to a compact 3.2×2.9 mm^2 MEMS chip for packaging in the endomicroscope, Fig 4. We fabricated the chip holder from M3 crystal, an acrylic based resin with high strength and stiffness, using a high precision 3D printer (ProJet 3500HD MAX, 3DSystems) with 16 μm resolution. We inserted copper (Cu) pins at the edge of the holder for use as electrical contacts to deliver power. Copper wires were used to deliver the drive signals to the MEMS chip, and aluminium (Al) wires were used between the Cu pins and the scanner [22].

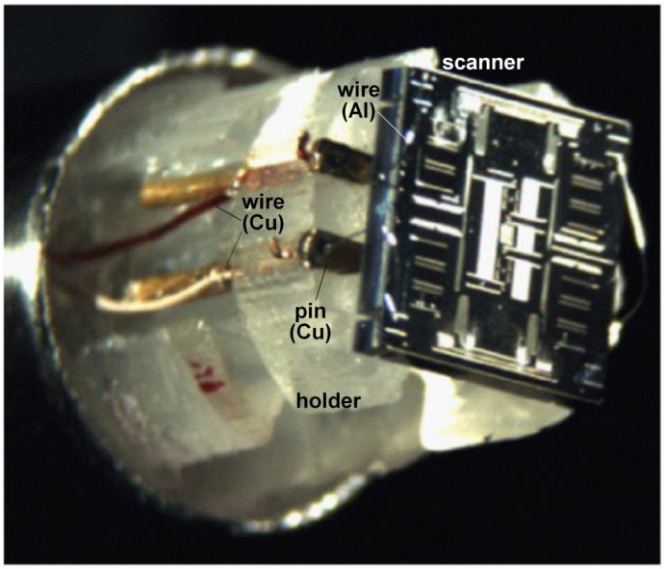

Fig. 4. Scanner packaging. Device is secured on a MEMS chip mounted to a M3 crystal holder. Electrical connections are provided using aluminum (Al) wired delivered via copper (Cu) pins and wires to the high voltage source.

E. Alignment of optics

We used an uncoated stainless steel tube with an outer diameter (OD) of 5.5 mm and an inner diameter (ID) of 5.0 mm to house the dual axes scanhead, Fig. 5. We used an iterative process to align the optics by maximizing the overlap of the intersecting focal volume between the two beams for optimal lateral and axial resolution. We first used a beam analysis system (BeamScan XYS, Ophir Photonics) to grossly align the two beams in a parallel configuration with an initial

This article has been accepted for publication in a future issue of this journal, but has not been fully edited. Content may change prior to final publication. Citation information: DOI 10.1109/TMI.2017.2673022, IEEE Transactions on Medical Imaging

accuracy of <0.27 mrad.

Two custom 0.1 degree optical wedges (Risley prisms) are inserted in the illumination path and rotated for fine alignment. The wedges (Tower Optical) are 1.2 mm in diameter, and are fabricated from N-BK7 glass with anti-reflection coating with reflectivity <0.5% between 640 and 785 nm to match the excitation and emission wavelengths of Cy5.5. By rotating the prisms, we can steer the illumination beam over a maximum range of 0.87 mrad. After alignment was completed, the positions of the two prisms were fixed with UV glue. We achieved a final accuracy for the lateral and axial positions of the illumination relative to the collection light path of 0.085 and 0.019 mrad, respectively.

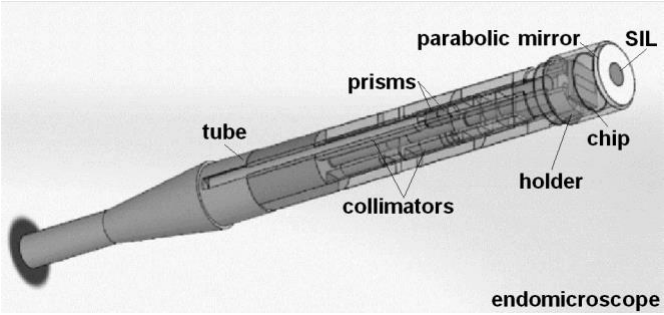

Fig. 5. Dual axes confocal endomicroscope. CAD drawing shows details for assembly and alignment of optics with integration of scanner.

F. *Measurement of resolution*

We measured the lateral resolution using the knife-edge method, where the distance that spans 10%-90% of maximum intensity across a border on a standard (USAF 1951) resolution target is determined. The axial resolution was measured by translating a plane mirror in the vertical direction at a working distance of 200 μm in scatter-free air film, and quantifying the full-width-at-half-maximum (FWHM).

G. *Collection of images*

All experimental procedures were performed in accordance with relevant guidelines and regulations of the University of Michigan, and the mouse imaging studies were conducted with approval by the University Committee on the Use and Care of Animals (UCUCA). We used 8 week-old *CPC;Apc* mice that have been genetically engineered to sporadically delete the APC gene and spontaneously develops colonic adenomas that overexpress EGFR [23]. The mice were housed in pathogen-free conditions and supplied water ad libitum under controlled conditions of humidity (50±10%), light (12/12 hour light/dark cycle) and temperature (25 ºC).

The dual axes confocal endomicroscope was positioned at normal incidence to the exposed mucosal surface of resected colon with the SIL in direct contact. NIR fluorescence images of adenoma and normal colon were collected in vertical and horizontal planes by tuning the drive frequency of the scanner. Videos were captured at 5 frames per second and exported in avi format with 8 bit (grayscale) digital resolution. Streams that showed minimum motion artifact and absence of debris (stool, mucus) were identified. The colon was then fixed in 10% buffered formalin and paraffin embedded for routine histology (H&E).

III. RESULTS

A. *MEMS scanner*

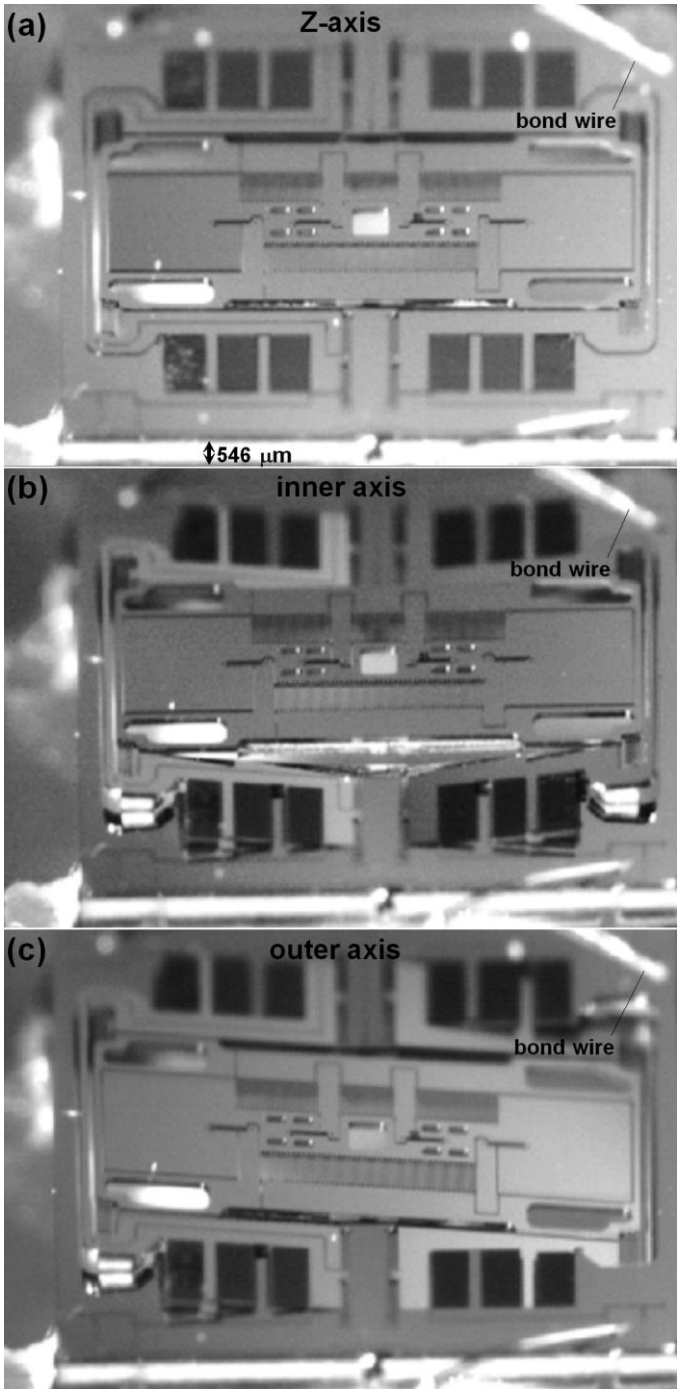

Fig. 6. Scanner displacement and deflection. (a) >400 μm out-of-plane motion of the mirror is shown with drive voltage of 60 V_{pp} and 25% duty cycle (Visualization1). The substrate has thickness of 546 μm, shown for comparison. (b) Large lateral deflections of the mirror along the inner axis at drive voltage of 50 V_{pp} and 50% duty cycle (Visualization2) and (c) outer axis at drive voltage of 60 V_{pp} and 50% duty cycle (Visualization3) are shown.

This article has been accepted for publication in a future issue of this journal, but has not been fully edited. Content may change prior to final publication. Citation information: DOI 10.1109/TMI.2017.2673022, IEEE Transactions on Medical Imaging

We produced compact monolithic 3D scanners using a robust silicon-on-insulator (SOI) micromachining process with a yield of >95%.

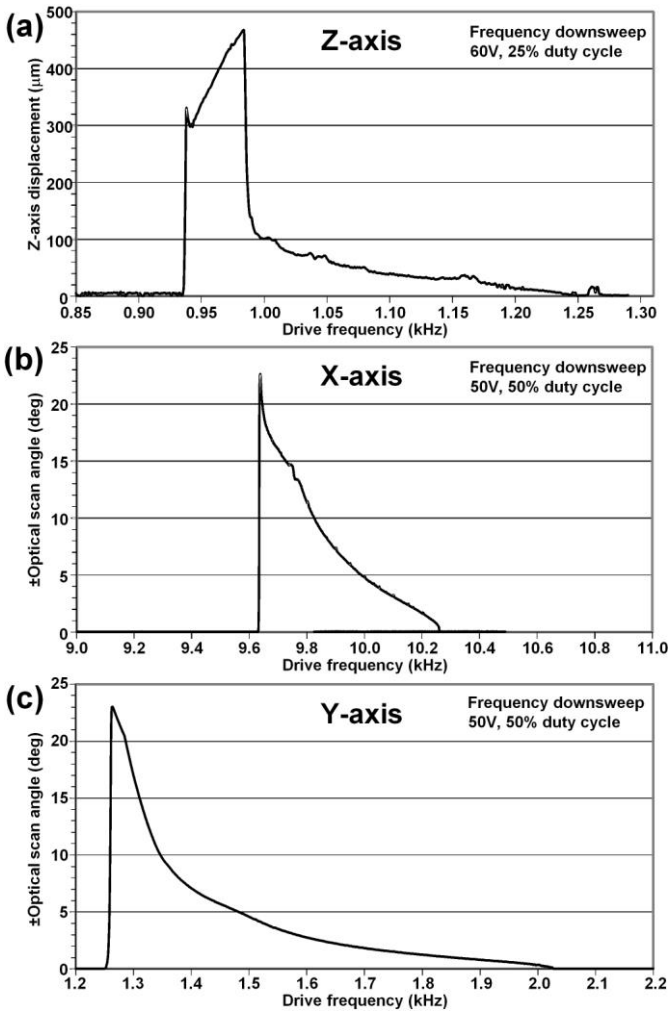

Fig. 7. Frequency response of scanner. (a) The magnitude of the out-of-plane mirror displacement in the Z-axis with a square wave drive voltage of 60 V_{pp}, 30V dc bias, and 25% duty cycle is shown versus drive frequency. Large lateral deflections of the mirror along the (b) inner axis with square wave drive voltage of 50 V_{pp}, 25V dc bias, and 50% duty cycle, and (c) outer axis with square wave drive voltage of 60 V_{pp}, 30V dc bias, and 50% duty cycle are shown versus drive frequency.

Drive signals applied to the electrostatic comb-drive actuators can instantaneously "switch" between large axial displacements, Fig. 6a (Visualization1), and wide lateral deflections in the inner, Fig. 6b (Visualization2), and outer axes, Fig. 6c (Visualization3).

We measured the frequency response of the scanner. The monolithic scanner provides an axial displacement of ~460 μm and optical scan angles of ±22.5° in the X-axis, ±23.0° in the Y-axis, Fig. 7. These large motions are produced by a non-linear response resulting from a complex interaction of electrostatic softening, mechanical hardening, and structural damping in the springs [18].

We measured the frequency response of the scanner, Fig. 7. We achieved images with the expected FOV of 1000×430 μm^2 and 1000×1000 μm^2 in the vertical and horizontal planes, respectively, by tuning the frequency, voltage, and duty cycle of a square wave: 0.97 kHz, 60 V_{pp}, 25% duty cycle for Z-axis; 9.79 kHz, 50 V_{pp}, 50% duty cycle for the inner axis; and 1.33 kHz, 50 V_{pp}, 50% duty cycle for the outer axis. The drive signals were applied to the scanner via a high voltage amplifier. A dense Lissajous scan pattern with 100% coverage was created at 5 frames per sec.

B. Scanner packaging

The dual axes confocal endomicroscope has been scaled down in dimensions to 5.5 mm diameter, assembled, aligned and packaged. Use for imaging as a handheld instrument is shown, Fig. 8.

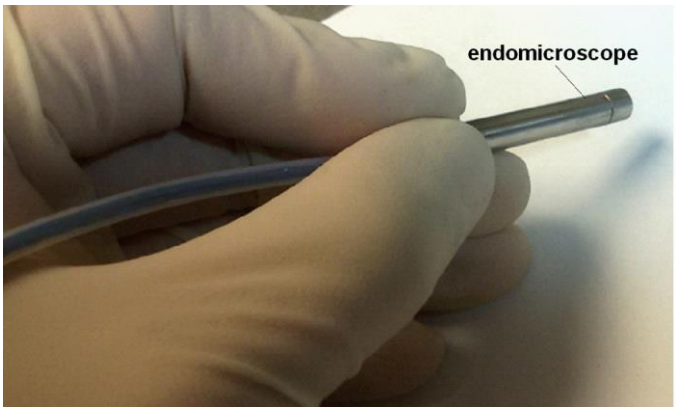

Fig. 8. The dual axes confocal endomicroscope has a dimeter of 5.5 mm and a rigid length of 38 mm for use as a handheld intra-vital imaging instrument.

The endomicroscope was inserted into the distal end of a medical endoscope with a 6 mm diameter biopsy channel for future in vivo imaging, Fig. 9.

Fig. 9. Dual axes confocal endomicroscope can be passed through the 6 mm diameter biopsy channel of a medical endoscope (Olympus GIF XTQ180).

C. Measurement of resolution

From our simulations using commercially-available lenses, we expect a lateral and axial resolution of 2.5 and 4.0 μm, respectively, and from diffraction theory with ideal lenses, we calculated 2.2 and 3.9 μm, respectively [24]. We measured a lateral resolution of 2.49 μm, defined by 10%-90% of

This article has been accepted for publication in a future issue of this journal, but has not been fully edited. Content may change prior to final publication. Citation information: DOI 10.1109/TMI.2017.2673022, IEEE Transactions on Medical Imaging

maximum intensity from a knife-edge target, Fig. 10a, and an axial resolution of 4.98 μm, defined by the full-width-at-half-maximum (FWHM), Fig. 10b. These results agree with theoretical and simulated values. We confirmed the lateral resolution with the mirror scanning using a standard resolution target (USAF 1951).

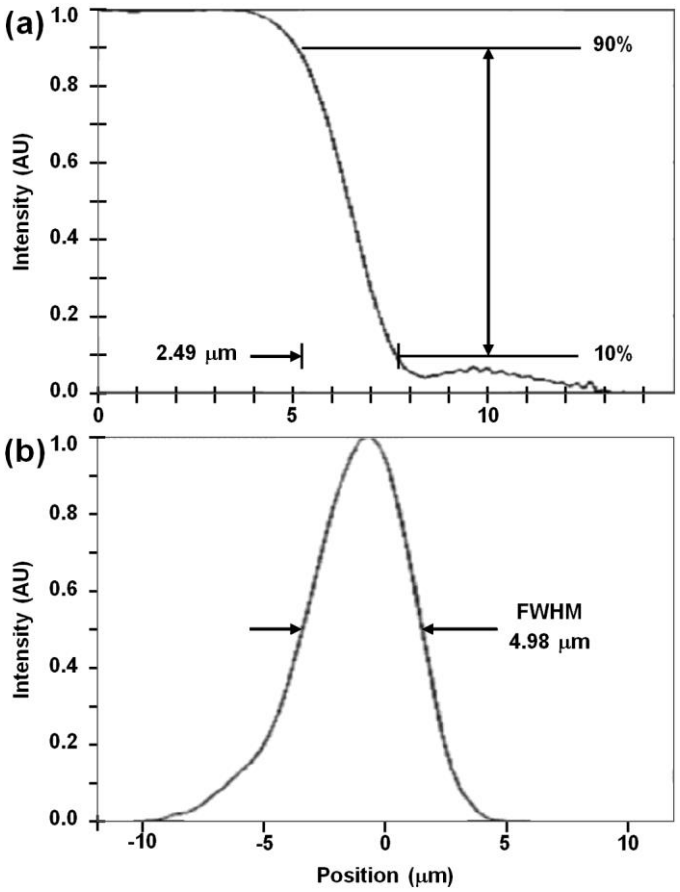

Fig. 10. Image resolution. (a) Lateral (10-90% of peak value) result of 2.49 μm, and (b) axial (FWHM) value of 4.98 μm were measured.

D. Collection of images in vertical plane

We have previously identified a peptide specific for domain 2 of EGFR [25]. This cell surface target is overexpressed in up to 80% of human colonic adenomas [26], and is important in the development and treatment of colorectal cancer [27]. We synthesized the monomeric linear peptide QRHKPRE, hereafter QRH*, with linker GGGSK using standard Fmoc-mediated solid-phase synthesis [28]. The Cy5.5 fluorophore was used as a label by coupling QRH* with water soluble sulfo-Cy5.5-N-hydroxysuccinimide ester (Lumiprobe LLC). Prior to use, the peptides were reconstituted in water at a concentration of 300 μM.

The dual axes confocal endomicroscope was placed in direct contact with the exposed mucosal surface of resected mouse colon to acquire optical sections of EGFR expression in pre-cancerous crypts. NIR confocal fluorescence images of colonic adenomas were collected in vertical planes. This view of adenoma shows a large number of crypt profiles near the epithelial surface compared with basally. The increased intensity reflects high levels of EGFR expression, Fig. 11a (Visualization4). These features are consistent with corresponding histology (H&E) for adenoma, Fig. 11b.

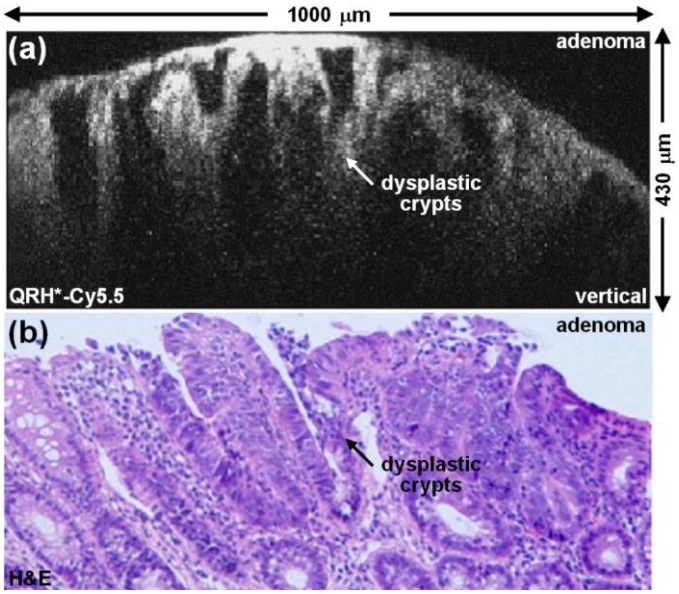

Fig. 11. Optical section of adenoma in vertical plane. (a) NIR confocal fluorescence image of EGFR expression from colonic adenoma (Visualization4) was collected with 430 μm depth at 90 minutes after intravenous injection of Cy5.5-labeled peptide. (b) Corresponding histology (H&E).

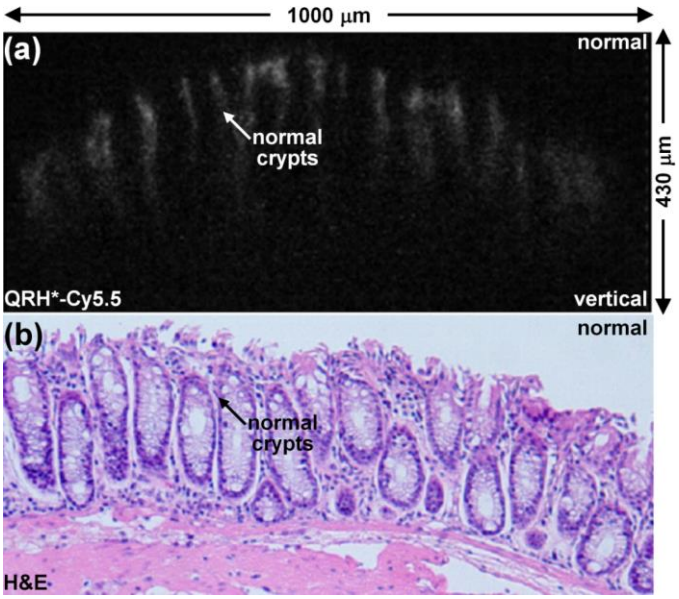

Fig. 12. Optical section of normal colon in vertical plane. (a) NIR confocal fluorescence image of EGFR expression from normal colonic mucosa (Visualization5) was collected with 430 μm depth 90 minutes after intravenous injection of Cy5.5-labeled peptide. (b) Corresponding histology (H&E).

NIR confocal fluorescence images of normal colon were also collected in vertical planes. Faint signal is seen for normal mucosa, and reveals low levels of EGFR expression, Fig. 12a. Crypts are uniform in size, evenly spaced, and lined by tall columnar epithelium with numerous goblet cells (Visualization5). These features are consistent with

This article has been accepted for publication in a future issue of this journal, but has not been fully edited. Content may change prior to final publication. Citation information: DOI 10.1109/TMI.2017.2673022, IEEE Transactions on Medical Imaging

corresponding histology (H&E) for normal, Fig. 12b.

E. Collection of images in horizontal plane

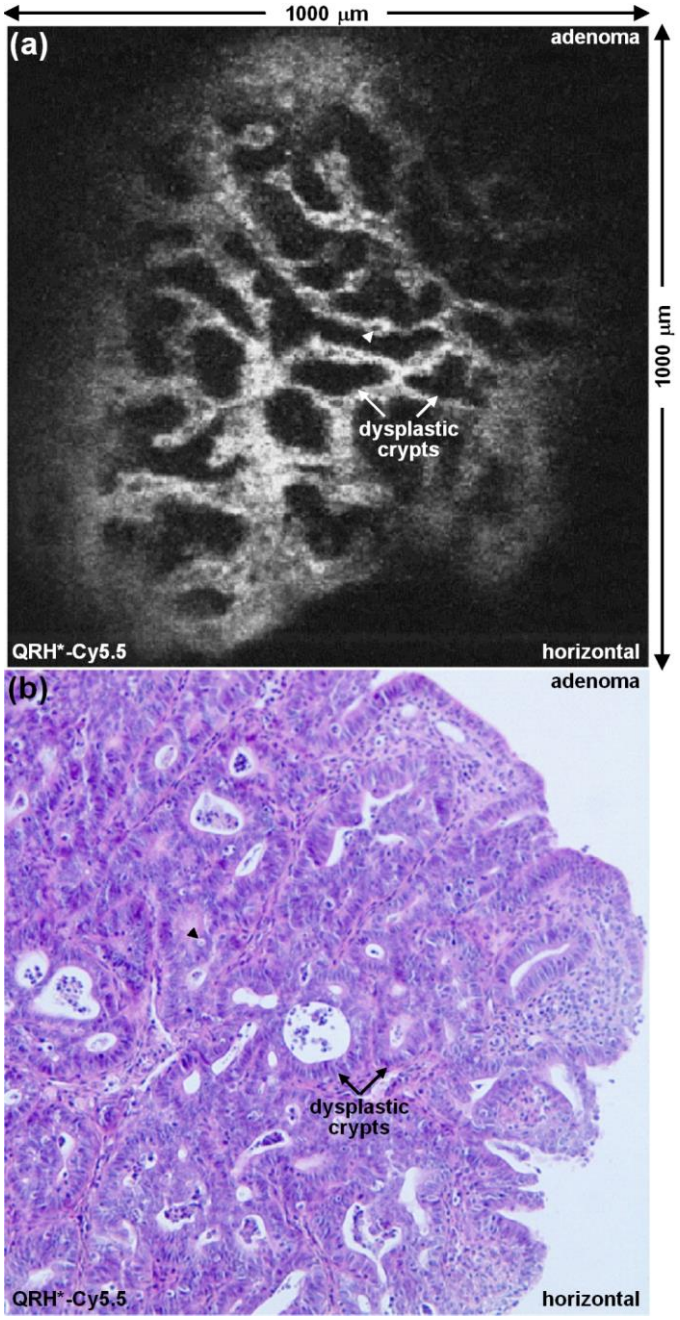

Fig. 13. Optical section of adenoma in horizontal plane. a) NIR confocal fluorescence image of EGFR expression from colonic adenoma (Visualization6) was collected at a depth of 50 μm at 90 minutes after intravenous injection of the Cy5.5-labeled peptide. Dysplastic crypts (arrows) and goblet cells (arrowheads) can be appreciated. (b) Corresponding histology (H&E).

The imaging mode was "switched" to collect optical sections in the horizontal plane by tuning the parameters of the drive signals to the scanner. NIR confocal fluorescence images of colonic adenomas were collected in the horizontal planes with a FOV of 1000×1000 μm^2 at a depth of 50 μm. In this view of the adenoma, we observed irregular crypt architecture with few goblet cells, Fig. 13a (Visualization6). These features are consistent with corresponding histology (H&E) for adenoma, Fig. 13b.

NIR confocal fluorescence images of normal colonic mucosa were collected in the horizontal plane with a FOV of 1000×1000 μm^2 at a depth of 50 μm, Fig. 14a (Visualization7). We observed minimal staining, and the crypts appeared circular in shape with uniform dimensions. These features are consistent with corresponding histology (H&E) for normal, Fig. 14b.

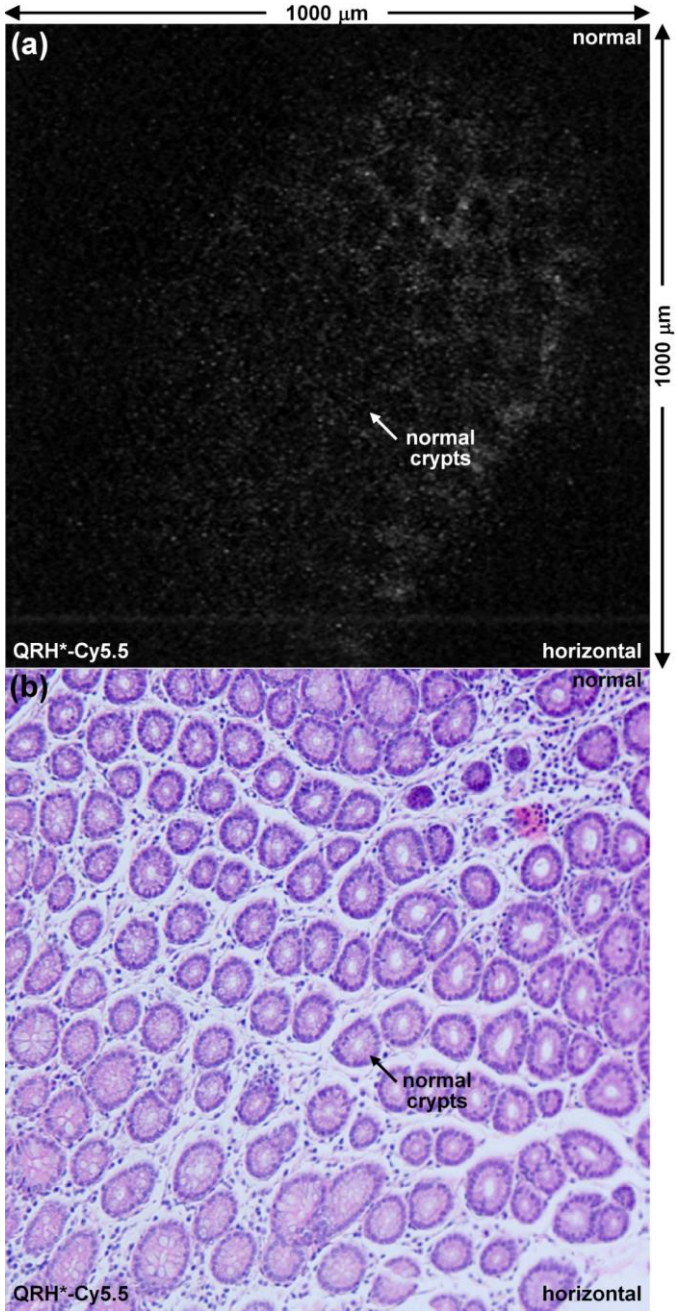

Fig. 14. Optical section of normal colonic mucosa in horizontal plane. (a) NIR confocal fluorescence image of EGFR expression from normal colonic mucosa (Visualization7) was collected at a depth of 50 μm at 90 minutes after intravenous injection of the Cy5.5-labeled peptide. (b) Corresponding histology (H&E).

This article has been accepted for publication in a future issue of this journal, but has not been fully edited. Content may change prior to final publication. Citation information: DOI 10.1109/TMI.2017.2673022, IEEE Transactions on Medical Imaging

IV. DISCUSSION6

Here, we demonstrate use of a fast, compact monolithic scanner fabricated using microelectromechanical systems (MEMS) technology located in the distal end of an endomicroscope. The dual axes configuration provides a high dynamic range needed to collect optical sections of NIR fluorescence in the vertical plane with an imaging depths >430 μm at 5 frames per sec. This depth is adequate to visualize important biological processes that occur in the epithelium, such as tissue differentiation, vessel formation, barrier function, and self-renewal [29], and the imaging speed is sufficient for future in vivo imaging. In the post-objective location [30], the scanner was able to produce wide angular deflections >20^o to achieve a FOV of 1000×1000 μm^2 in the horizontal plane. This result is much larger than that of other endomicroscopes with similar dimensions [2,3], including our previous 5.5 mm diameter instrument, which achieved a FOV of only 362×212 μm^2 [31].

We used a MEMS-based scanner that combines torsional and serpentine springs using a design based on the mechanism of parametric resonance in a monolithic device. By attaching the springs to a gimbal frame linked to a U-shaped suspension, we were able to switch the scan direction between vertical and horizontal planes to provide a more complete view of the epithelium. Large out-of-plane motions and wide angular deflections were achieved using drive voltage <60 V_{pp}. Electrical isolation is achieved by containing the scanner inside a stainless steel tube. We found the scanner to work reliably after packaging, and were able to collect images continuously for several hours. The device consistently "switched" imaging modes at fixed drive frequencies without noticeable phase shifts. Horizontal and vertical stacks can be generated to produce 3-dimensional volumetric images, representing a key advance in endomicroscopy technology that is currently limited to imaging in horizontal planes only at fixed depths.

This device represents a significant improvement in imaging performance compared with other MEMS scanners used in the dual axes confocal endomicroscope. The previous 5.5 mm diameter instrument used a MEMS scanner to perform fast lateral scanning to achieve a FOV of 362×212 μm^2 at 5 frames per sec. A dc micromotor was used to drive a linear actuator to achieve an imaging depth of 140 μm [31]. In a later version, a computer controlled piezoelectric micromotor was used to improve the imaging depth to 300 μm [32]. Vertical cross-sections were created by collecting a Z-stack of horizontal images and using post-processing to create a 3D volumetric image. By comparison, we were able to achieve >10-fold larger FOV at the same imaging speed and a factor of 3 greater imaging depth. Deformable metallized polymer membranes are also promising as MEMS devices, but only 85 μm axial displacement has been demonstrated so far [33]. The scanner appears to work reliably. We were able to collect images in tissue for several hours at a time, and have operated some scanners continuously for up to 5 days. Some of our systems have lasted over 6 months.

Shape memory alloys were used in first generation single axis confocal endomicroscopes to provide axial large displacement of 250 μm, but this approach is slow and suffers from hysteresis [2]. Electrothermal devices can provide large axial displacements at low voltages, but have high power dissipation requirements and have not yet been incorporated into endomicroscopes [34]. Electromagnetic scanners have been developed with fast response times and good vertical displacements, however, this technology is challenging to scale down in size to an endomicroscopic form factor [35]. Piezoelectric actuators can achieve large vertical displacements in a small form factor, but may not have the speed needed to perform fast lateral scanning [36].

Currently, clinical confocal endomicroscopes image in horizontal planes only and use contrast generated from intravenously injected dyes, such as fluorescein [37]. These dyes follow a vascular distribution and are non-specific for disease. We visualized molecular expression in both vertical and horizontal planes by using a peptide to target EGFR expressed in pre-malignant colonic epithelium. Peptide have small size and low molecular weight by comparison to antibodies for improved vascular permeability and more effective targeting with deep tissue imaging in the vertical plane [38]. By using a non-refractive focusing element (parabolic mirror) to avoid chromatic dispersion, we can also detect multiple targets at the same time using additional lasers and fluorophores [39]. Other targeting moieties, including enzyme activatable [40], antibodies [41], vitamins [42], and lectins [43], are being developed to image biological function. This integrated approach can potentially serve as an adjunct to medical endoscopy by visualizing molecular expression of disease targets for real time pathology in the epithelium of hollow organs and to guide point-of-care diagnostics.

V. CONCLUSIONS

We present an endoscope-compatible dual axes confocal endomicroscope with a compact, monolithic scanner located in the post-objective position. Optical sections of epithelium were collected in vertical and horizontal planes with sub-cellular resolution at 5 frames per sec. We demonstrate ex vivo near-infrared fluorescence images that target overexpressed EGFR in pre-cancerous mouse colon with 430 μm vertical depth and 1×1 mm^2 horizontal area using a systemically administered Cy5.5-labeled peptide. The instrument dimensions are compatible with the biopsy channel of medical endoscopes to allow for future in vivo imaging.

ACKNOWLEDGMENT

We thank Jin Gao and Zhenzhen Dai for technical support.

REFERENCES

[1] Pawley, J. B. Handbook of Biological Confocal Microscopy 3rd ed (Springer, Berlin, 2006).

[2] Kiesslich R, Burg J, Vieth M, Gnaendiger J, Enders M, Delaney P, Polglase A, McLaren W, Janell D, Thomas S, Nafe B, Galle PR, Neurath MF. Confocal laser endoscopy for diagnosing intraepithelial neoplasias and colorectal cancer in vivo. Gastroenterology 2004;127:706-13.

[3] Wang TD, Friedland S, Sahbaie P, Soetikno R, Hsiung PL, Liu JT, Crawford JM, Contag CH. Functional imaging of colonic mucosa with a fibered confocal microscope for real-time in vivo pathology. Clin

Gastroenterol Hepatol 2007;5):1300-5.
[4] Clevers H. The intestinal crypt, a prototype stem cell compartment. Cell 2013;154:274-84.
[5] Hanahan D, Weinberg RA. The hallmarks of cancer. Cell 2000;100:57-70.
[6] Wang TD, Van Dam J, Crawford JM, Preisinger EA, Wang Y, Feld MS. Fluorescence endoscopic imaging of human colonic adenomas. Gastroenterology 1996;111:1182-91.
[7] Torre LA, Bray F, Siegel RL, Ferlay J, Lortet-Tieulent J, Jemal A. Global cancer statistics, 2012. CA Cancer J Clin 2015;65:87-108.
[8] Dolak W, Mesteri I, Asari R, Preusser M, Tribl B, Wrba F, Schoppmann SF, Hejna M, Trauner M, Häfner M, Püspök A. A pilot study of the endomicroscopic assessment of tumor extension in Barrett's esophagus-associated neoplasia before endoscopic resection. Endosc Int Open 2015;3:E19-28.
[9] Baak JP, ten Kate FJ, Offerhaus GJ, van Lanschot JJ, Meijer GA. Routine morphometrical analysis can improve reproducibility of dysplasia grade in Barrett's oesophagus surveillance biopsies. J Clin Pathol 2002;55:910-6.
[10] Karstensen JG, Klausen PH, Saftoiu A, Vilmann P. Molecular confocal laser endomicroscopy: a novel technique for in vivo cellular characterization of gastrointestinal lesions. World J Gastroenterol 2014;20:7794-800.
[11] Tontini GE, Mudter J, Vieth M, Atreya R, Günther C, Zopf Y, Wildner D, Kiesslich R, Vecchi M, Neurath MF, Neumann H. Confocal laser endomicroscopy for the differential diagnosis of ulcerative colitis and Crohn's disease: a pilot study. Endoscopy 2015;47:437-43.
[12] Kiesslich R, Gossner L, Goetz M, Dahlmann A, Vieth M, Stolte M, Hoffman A, Jung M, Nafe B, Galle PR, Neurath MF. In vivo histology of Barrett's esophagus and associated neoplasia by confocal laser endomicroscopy. Clin Gastroenterol Hepatol 2006;4:979-87.
[13] Mandella M. J., Wang T. D. Dual Axes Confocal Microscopy. In: Tuchin VV Ed. Handbook of Photonics for Medical Science (CRC Press, London, UK 2010) pp 481-508.
[14] Wong LK, Mandella MJ, Kino GS, Wang TD. Improved rejection of multiply scattered photons in confocal microscopy using dual-axes architecture, Optics Letters 2007;32:1674-6.
[15] Qiu Z, Liu Z, Duan X, Khondee S, Joshi BP, Mandella MJ, Oldham K, Kurabayashi K, Wang TD. Targeted vertical cross-sectional imaging with handheld near-infrared dual axes confocal fluorescence endomicroscope. Biomedical Optics Express 2013;4:322-330.
[16] Kwon S, Milanovic V, Lee LP. Large-displacement vertical microlens scanner with low driving voltage, IEEE Photon. Technol. Lett. 2002;14:1572–1574.
[17] Chiou JC, Kou CF, Lin YJ, A micromirror with large static rotation and vertical actuation, IEEE J Sel Topics Quantum Electron 2007;13:297–303.
[18] Liu L, Wang E, Zhang X, Liang W, Li X, Xie H. MEMS-based 3D confocal scanning microendoscope using MEMS scanners for both lateral and axial scan. Sensors and Actuators A: Physical 2014;215:89-95.
[19] Li H, Qiu Z, Duan X, Oldham K, Kurabayashi K, Wang TD. A Monolithically-Integrated 3D MEMS Scanner for Switchable Real-time Vertical/Horizontal Cross-sectional Imaging in Dual Axes Confocal Endomicroscope. Optics Express 2016;24:2145-55.
[20] Turner KL, Miller SA, Hartwell PG, MacDonald NC, Strogatz SH, Adams SG. Five parametric resonances in a microelectromechanical system, Nature 1998;396:149-152.
[21] Shahid W, Qiu Z, Duan X, Li H, Wang TD, Oldham KR. Modeling and Simulation of a Parametrically Resonant Micro-Mirror with Duty-Cycled Excitation. IEEE J of Microelectromechanical Systems 2014;23:1440-53.
[22] Duan X, Li H, Qiu Z, Joshi BP, Pant A, Smith A, Kurabayashi K, Oldham KR, Wang TD. MEMS-based multiphoton endomicroscope for repetitive imaging of mouse colon. Biomed Opt Express 2015;6:3074-83.
[23] Hinoi T, Akyol A, Theisen BK, Ferguson DO, Greenson JK, Williams BO, Cho KR, Fearon ER. Mouse model of colonic adenoma-carcinoma progression based on somatic Apc inactivation. Cancer Res 2007;67:9721-30.
[24] Piyawattanametha W., Wang T. D. In Vivo Microendoscopy. In: Tunnell J Ed. In Vivo Clinical Imaging and Diagnosis (McGraw Hill Professional, New York, NY 2011) 45-76.
[25] Zhou J, Joshi BP, Duan X, Pant A, Qiu Z, Kuick R, Owens SR, Wang TD. EGFR Overexpressed in Colonic Neoplasia Can be Detected on Wide-Field Endoscopic Imaging. Clin Transl Gastroenterol 2015;6:e101.
[26] Rowan AJ, Lamlum H, Ilyas M, Wheeler J, Straub J, Papadopoulou A, Bicknell D, Bodmer WF, Tomlinson IP.APC mutations in sporadic colorectal tumors: A mutational "hotspot" and interdependence of the "two hits". Proc Natl Acad Sci 2000;97:3352-7.
[27] Van Cutsem E, Köhne CH, Hitre E, Zaluski J, Chang Chien CR, Makhson A, D'Haens G, Pintér T, Lim R, Bodoky G, Roh JK, Folprecht G, Ruff P, Stroh C, Tejpar S, Schlichting M, Nippgen J, Rougier P.Cetuximab and chemotherapy as initial treatment for metastatic colorectal cancer. N Engl J Med 2009;360:1408-17.
[28] Fields G.B. and Noble R.L. Solid phase peptide synthesis utilizing 9-fluorenylmethoxycarbonyl amino acids. Int J Pept Protein Res 1990;35:161-214.
[29] Barker N, Ridgway RA, van Es JH, van de Wetering M, Begthel H, van den Born M, Danenberg E, Clarke AR, Sansom OJ, Clevers H. Crypt stem cells as the cells-of-origin of intestinal cancer. Nature 2009;457:608-11.
[30] Wang TD, Mandella MJ, Contag CH, Kino GS. Dual Axes Confocal Microscope with Post-Objective Scanning and Low Coherence Heterodyne Detection. Optics Letters 2003;28:1915-17.
[31] Piyawattanametha W, Ra H, Qiu Z, Friedland S, Liu JTC, Loewke K, Kino GS, Solgaard O, Wang TD, Mandella MJ, Contag CH. In vivo near-infrared dual-axis confocal microendoscopy in the human lower gastrointestinal tract, J Biomedical Optics 2012:17:021102.
[32] Piyawattanametha W, Ra H, Mandella MJ, Loewke K, Wang TD, Kino GS, Solgaard O, Contag CH. 3-D Near-Infrared Fluorescence Imaging Using an MEMS-Based Miniature Dual-Axis Confocal Microscope, IEEE J Sel Topics Quantum Electronics 2009;15:1344-50.
[33] Moghimi MJ, Lutzenberger BJ, Kaylor BM, Dickensheets DL. MOEMS deformable mirrors for focus control in vital microscopy. J. Micro/Nanolith. MEMS MOEMS2011;10, 023005.
[34] Wu L, Xie H. A large vertical displacement electrothermal bimorph microactuator with very small lateral shift. Sensors and Actuators A: Physical 2010;145-46;371-79.
[35] Mansoor H, Zeng H; Tai IT, Zhao J; Chiao M. A Handheld Electromagnetically Actuated Fiber Optic Raster Scanner for Reflectance Confocal Imaging of Biological Tissues. IEEE Transactions on Biomedical Engineering 2013;60:1431-38.
[36] Domke J, Rhee CH, Liu Z, Wang TD, Oldham KR. Amplifying transmission and compact suspension for a low profile, large displacement piezoelectric microactuator, J Micromechanics Microengineering 2011;21:067004.
[37] Wallace MB, Meining A, Canto MI, Fockens P, Miehlke S, Roesch T, Lightdale CJ, Pohl H, Carr-Locke D, Löhr M, Coron E, Filoche B, Giovannini M, Moreau J, Schmidt C, Kiesslich R. The safety of intravenous fluorescein for confocal laser endomicroscopy in the gastrointestinal tract. Aliment Pharmacol Ther 2010;31:548-52.
[38] Lee S, Xie J, Chen X. Peptides and peptide hormones for molecular imaging and disease diagnosis. Chem Rev 2010;110:3087-111.
[39] Qiu Z, Khondee S, Duan X, Li H, Mandella MJ, Joshi BP, Zhou Q, Owens SR, Kurabayashi K, Oldham K, Wang TD. Vertical cross-sectional imaging of colonic dysplasia in vivo with multi-spectral dual axes confocal endomicroscopy. Gastroenterology 2014;146:615-17.
[40] Mahmood U, Weissleder R. Near-infrared optical imaging of proteases in cancer. Mol Cancer Ther 2003;2:489-96.
[41] Atreya R, Neumann H, Neufert C, Waldner MJ, Billmeier U, Zopf Y, Willma M, App C, Münster T, Kessler H, Maas S, Gebhardt B, Heimke-Brinck R, Reuter E, Dörje F, Rau TT, Uter W, Wang TD, Kiesslich R, Vieth M, Hannappel E, Neurath MF. In vivo imaging using fluorescent antibodies to tumor necrosis factor predicts therapeutic response in Crohn's disease. Nat Med 2014;20:313-8.
[42] van Dam GM, Themelis G, Crane LM, Harlaar NJ, Pleijhuis RG, Kelder W, Sarantopoulos A, de Jong JS, Arts HJ, van der Zee AG, Bart J, Low PS, Ntziachristos V. Intraoperative tumor-specific fluorescence imaging in ovarian cancer by folate receptor-α targeting: first in-human results. Nat Med 2011;17:1315-9.
[43] Bird-Lieberman EL, Neves AA, Lao-Sirieix P, O'Donovan M, Novelli M, Lovat LB, Eng WS, Mahal LK, Brindle KM, Fitzgerald RC. Molecular imaging using fluorescent lectins permits rapid endoscopic identification of dysplasia in Barrett's esophagus. Nat Med 2012;18:315-21.